

## TURBULENCE MODELS EVALUATION WITH RESPECT TO THE PREDICTION OF THE BACKSTEP PROBLEM

**Arturo Jesus Ortega Malca**

Dept. Mech. Eng., PUC-Rio, tupamaru@mec.puc-rio.br

**Daniel Irigon de Irigon**

Dept. Mech. Eng., PUC-Rio, dirigon@mec.puc-rio.br

**Erick Fabrizio Quintela Andrade Coelho**

Dept. Mech. Eng., PUC-Rio, erick@mec.puc-rio.br

**Luiz Eduardo Bittencourt Sampaio**

Dept. Mech. Eng., PUC-Rio, luizebs@mec.puc-rio.br

**Miguel Angel Tupa Walter**

Dept. Mech. Eng., PUC-Rio, mwalter@mec.puc-rio.br

**Reginaldo Rosa Couto de Paula**

Dept. Mech. Eng., PUC-Rio, rcotto@bol.com.br

**Angela Ourivio Nieckele**

Department of Mechanical Engineering, Pontifical Catholic University of Rio de Janeiro, 22453-900 – Rio de Janeiro, RJ, Brazil  
nieckele@mec.puc-rio.br

***Abstract.** The classical backstep problem is investigated applying six different turbulence models. Two version of the one equation turbulent model of Spalart-Allmaras were selected. The first one considers turbulence production based only on vorticity, while the second one considers both vorticity and deformation. The other four models are two equation models, the  $\kappa$ - $\omega$  model of Wilcox and three variants of the  $\kappa$ - $\epsilon$  turbulence model: the tradition  $\kappa$ - $\epsilon$  model with wall-law, a low Reynolds number  $\kappa$ - $\epsilon$  model and a RNG  $\kappa$ - $\epsilon$  model. Due to the abundance of data regarding the backstep geometry, it was selected to be tested. The objective of the analysis is to identify which are the favorable and non-favorable characteristics of each model, to help the selection of the appropriate model for different applications. The ability of capturing the recirculation areas, pressure recovery after the obstruction, and shear distribution is investigated. The fields of velocity, turbulent kinetic energy, dissipation rate obtained by the different models are compared with numerical and experimental data found in the literature.*

***Keywords.** Turbulence models, backstep problem, computational analysis*

### 1. Introduction

The study of the turbulent flow with separation, recirculation and reattachment has been a subject of fundamental fluid engineering research during the last years. The occurrence of these phenomena may affect fundamental flow characteristics, resulting in drastic changes on the performance of fluid machinery. Within this framework, the flow past a backward-facing step has attracted considerable attention. The flow over a backward-facing step consists of different complex flow regimes, which includes flow separation and subsequent reattachment due to a sudden expansion in the flow geometry, reversal and recovery in the presence of adverse pressure gradient and Kelvin-Helmholtz type instability (Silveira Neto, 2002). A main recirculation zone is formed adjacent to the step due to the separation at the corner of the step (Kung, et al., 2003). How or where the separation starts and develops to a recirculating flow pattern are the major concerns of this classical field.

Due to the interest in the flow dynamics over backward-facing step (BFS), a considerable amount of work employing various measurement techniques (Eaton and Johnston, 1981; Tylli et al., 2002) and numerical simulation (Silveira Neto et al, 1993; Le et al., 1997, Bredberg et al., 2002 ) can be found in the literature. Lee and Mateescu (1998) carried an experimental and numerical investigation of air flow over a BFS to identify laminar and transitional flow regimes, for  $Re \leq 3000$  with expansion ratios of 1.7 and 2.0. The numerical method used in the study was based on a finite difference formulation and used an artificial compressibility approach. The result showed that, the locations of flow separation and reattachment points on the upper and lower wall of the 2-D channel can be obtained both non-intrusively and simultaneously. The multiple hot-film sensor measurements were found to be in good agreement with the numerical predictions. The authors pointed that due to presence of a reverse flow, conventional surface pressure measurement and hot-wire arrays cannot conveniently be used in this region. Avancha and Pletcher (2002) presented a study of the heat transfer and fluid mechanics of the turbulent separating and reattaching flow past a BFS using large eddy simulation. The result showed that the viscous sub-layer played a critical role in controlling the heat transfer rate. Streamwise and wall-normal turbulent heat flux, were of the same order of magnitude.

The advent of high performance computers in recent decades, coupled with the development of various turbulence models, like Spalart-Allmaras model (1992),  $\kappa$ - $\omega$  model of Wilcox (1988) and  $\kappa$ - $\epsilon$  eddy viscosity models (Jones and Launder (1972)), have allowed successful applications of computational fluid dynamics (CFD) in engineering situations. However, continuous evaluation and development of turbulence models are still representing a necessity to help in the selection of the appropriate model for different applications. The present paper evaluates and compares six different turbulence models: Spalart Allmaras models (Spalart-I) vorticity-based-production, Spalart-Allmaras strain/vorticity-based production (Spalart-II), traditional  $\kappa$ - $\epsilon$  model with wall function ( $\kappa$ - $\epsilon$  I), and with a non-equilibrium wall function ( $\kappa$ - $\epsilon$  II) and the  $\kappa$ - $\epsilon$  RNG model and  $\kappa$ - $\omega$  model of Wilcox, when applied to the turbulent flow over a backward-facing step, using FLUENT code. The objective of this work is to investigate the ability of the turbulence models to capture the recirculation region, pressure recovery after obstruction and shear distribution. The obtained results were compared with the results of direct numerical simulation by Le et al. (1997) and experimental data by Jovic and Driver (1994).

## 2. Mathematical Modeling

The present situation corresponds to a turbulent flow of an incompressible fluid, through a flat plate channel with double expansion, as illustrated in Fig. 1. The  $x$  axis is taken in the main flow direction and the  $y$  axis in the vertical direction. The origin of the coordinate system is located at a position on the bottom step. The computational domain consist of a streamwise length  $L_x = 30h$ , including an inlet section,  $L_i = 10h$  prior to the sudden expansion, vertical height  $L_y = 6h$ , where  $h$  is the step height (Le et al., 1997), with  $h = 1$  cm. Therefore, the expansion ratio  $ER = L_y / (L_y - h)$  is 1.2 in agreement with the work by Le et al. (1997). The flow was modeled as two-dimensional, and due to symmetry, the flow was solved in only one-half of the domain. The step-height Reynolds number, defined as  $Re_h = U_0 h / \nu$ , where  $\nu$  is the kinematic viscosity and  $U_0$  being the centerline mean inlet velocity, was taken as 5100.

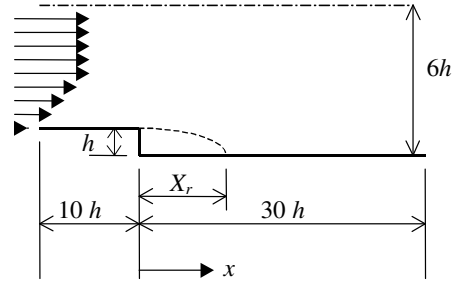


Figure1. Backstep geometry

The inlet time average velocity profile was obtained from a boundary layer velocity profile, being a function of the boundary layer thickness  $\delta$  as

$$U(y) = \mathbf{Re}_h (\nu/h) (y/\delta)^{1/5.8} \quad \delta = [(1.2h)^{5/4} - 3.175 h (h/\mathbf{Re}_h)^{1/4}]^{1/5} \quad (1)$$

It was assumed that the inlet turbulent intensity was equal to 1% of the mean flow kinetic energy, and an inlet characteristic length equal to 2.5% of the inlet flat plate distance ( $0.25 h$ ).

The time average continuity and linear momentum conservation equation are

$$\frac{\partial \bar{u}_i}{\partial x_i} = 0 \quad (2)$$

$$\frac{\partial \rho \bar{u}_j \bar{u}_i}{\partial x_j} = -\frac{\partial \bar{p}}{\partial x_i} + \frac{\partial}{\partial x_j} \left[ \mu \left( \frac{\partial \bar{u}_i}{\partial x_j} + \frac{\partial \bar{u}_j}{\partial x_i} \right) - \rho \overline{u_i' u_j'} \right] \quad (3)$$

where  $\bar{u}_i$  is the time average velocity component,  $\bar{p}$  is the pressure,  $\mu$  is the absolute viscosity, and  $-\rho \overline{u_i' u_j'}$  is the Reynolds stress, which can be modeled based on the Boussinesq hypothesis as

$$-\rho \overline{u_i' u_j'} = \mu_t \left( \frac{\partial \bar{u}_i}{\partial x_j} + \frac{\partial \bar{u}_j}{\partial x_i} \right) - \frac{2}{3} \rho \kappa \delta_{ij} \quad (4)$$

where  $\mu_t$  is the turbulence viscosity, taking different forms depending on the turbulence model.  $\kappa$  is the turbulent kinetic energy. The effective viscosity is  $\mu_{ef} = \mu + \mu_t$ .

### 2.1 Turbulence Models

The six different turbulence models tested are described next. Two variations of the Spalart Allmaras models were investigated. The first has a vorticity-based-production (SA-I) and the second one a strain/vorticity-based production (SA-II). The viscosity is given by

$$\mu_t = \rho \tilde{\nu} f_{v1} \quad f_{v1} = \chi^3 / (\chi^3 + C_{v1}^3) \quad \chi \equiv \tilde{\nu} / \nu \quad (5)$$

$$\frac{\partial(\rho \tilde{v})}{\partial t} + \frac{\partial(\rho \tilde{v} \bar{u}_i)}{\partial x_i} = C_{b1} \rho \tilde{S} \tilde{v} + \frac{1}{\sigma_{\tilde{v}}} \left[ \frac{\partial}{\partial x_j} \left\{ (\mu + \rho \tilde{v}) \frac{\partial \tilde{v}}{\partial x_j} \right\} + C_{b2} \rho \left( \frac{\partial \tilde{v}}{\partial x_j} \right)^2 \right] - C_{\omega 1} \rho f_{\omega} \left( \frac{\tilde{v}}{d} \right)^2 \quad (6)$$

$$\tilde{S} \equiv S + \frac{\tilde{v}}{k^2 d^2} \left[ 1 - \frac{\chi}{1 + \chi f_{v1}} \right] \quad S = |\Omega_{ij}| + C_{prod} \min \left( 0, |S_{ij}| - |\Omega_{ij}| \right) \quad (7)$$

$$|S_{ij}| = \sqrt{2 S_{ij} S_{ij}} \quad |\Omega_{ij}| = \sqrt{2 \Omega_{ij} \Omega_{ij}} \quad S_{ij} = \frac{1}{2} \left( \frac{\partial \bar{u}_j}{\partial x_i} + \frac{\partial \bar{u}_i}{\partial x_j} \right) \quad \Omega_{ij} = \frac{1}{2} \left( \frac{\partial \bar{u}_i}{\partial x_j} - \frac{\partial \bar{u}_j}{\partial x_i} \right) \quad (8)$$

$$c_{\omega 1} = \frac{c_{b1}}{k^2} + \frac{1 + c_{b2}}{\sigma_{\tilde{v}}} \quad f_{\omega}(g) = g \left( \frac{1 + c_{\omega 3}^6}{g^6 + c_{\omega 3}^6} \right)^{1/6} \quad g = r + c_{\omega 2} (r^6 - r) \quad r \equiv \frac{\tilde{\tau}}{\tilde{S} k^2 d^2} \quad (9)$$

where  $d$  is the distance to the wall, and the empirical constants are:  $c_{v1}=7.1$ ;  $k=0.4187$ ,  $c_{b1}=0.1355$ ;  $c_{b2}=0.662$ ;  $\sigma_{\tilde{v}}=2/3$ ;  $c_{\omega 2}=0.3$ ;  $c_{\omega 3}=2$ . For the first model, SA-I, the production depends only on the vorticity, thus  $C_{prod}=0$ , and for SA-II,  $C_{prod}=2$ . For these models, since  $\kappa$  is not known, the last term in eq. (3) is not considered to determine the Reynolds stresses.

The second set of turbulence models investigated, consisted on the traditional  $\kappa$ - $\varepsilon$  model and  $\kappa$ - $\varepsilon$  RNG model. The traditional  $\kappa$ - $\varepsilon$  model was applied with two different wall treatments: ( $\kappa$ - $\varepsilon$ -I) the traditional wall function and ( $\kappa$ - $\varepsilon$ -II) a non-equilibrium wall function depended on to pressure-gradient (Kim and Choudhury, 1995). The turbulent viscosity is given for these models as

$$\mu_t = \rho C_{\mu} \kappa^2 / \varepsilon \quad (10)$$

The conservation equations of the turbulent kinetic energy  $\kappa$  and its dissipation ratio  $\varepsilon$  are

$$\frac{\partial}{\partial x_j} (\rho \kappa \bar{u}_j) = \frac{\partial}{\partial x_j} \left[ \Gamma_{\kappa} \frac{\partial \kappa}{\partial x_j} \right] + G_{\kappa} - \rho \varepsilon \quad (11)$$

$$\frac{\partial}{\partial x_j} (\rho \varepsilon \bar{u}_j) = \frac{\partial}{\partial x_j} \left[ \Gamma_{\varepsilon} \frac{\partial \varepsilon}{\partial x_j} \right] + C_{1\varepsilon} \frac{\varepsilon}{\kappa} G_{\kappa} - C_{2\varepsilon} \rho \frac{\varepsilon^2}{\kappa} \quad (12)$$

$$G_{\kappa} = \mu_t \left( \frac{\partial \bar{u}_i}{\partial x_j} + \frac{\partial \bar{u}_j}{\partial x_i} \right) \frac{\partial \bar{u}_i}{\partial x_j} \quad \Gamma_{\kappa} = \mu + \mu_t / \sigma_{\kappa} \quad \Gamma_{\varepsilon} = \mu + \mu_t / \sigma_{\varepsilon} \quad (13)$$

The empirical constants of both  $\kappa$ - $\varepsilon$ -I and  $\kappa$ - $\varepsilon$ -II are:  $C_{\mu}=0.09$ ;  $C_{1\varepsilon}=1.44$ ;  $C_{2\varepsilon}=1.92$ ;  $\sigma_{\kappa}=1$ ;  $\sigma_{\varepsilon}=1$ . For the  $\kappa$ - $\varepsilon$  RNG, the empirical constants are:  $C_{\mu}=0.0845$ ;  $C_{1\varepsilon}=1.42$ ;  $C_{2\varepsilon}=1.68+R$ ;  $\sigma_{\kappa}=1.393$ ;  $\sigma_{\varepsilon}=1.393$ . The additional term  $R$  of the RNG  $\kappa$ - $\varepsilon$  model is given by

$$R = \frac{C_{\mu} \eta^3 (1 - \eta / \eta_0)}{1 + \beta \eta^3} \quad \eta \equiv |S_{ij}| \kappa / \varepsilon \quad \eta_0 = 4.38 \quad \beta = 0.012 \quad (14)$$

The traditional wall function employed for model  $\kappa$ - $\varepsilon$ -I can be summarized by

$$\begin{aligned} u^+ &= (1/k) \ln(E y^+) & y^+ &\geq 11.225 & u^+ &= u / u_{\tau} & u_{\tau} &= \sqrt{\frac{\tau_w}{\rho}} & \partial \kappa / \partial y &= 0 \\ u^+ &= y^+ & y^+ &< 11.225 & y^+ &= \rho u_{\tau} y / \mu & \varepsilon &= C_{\mu}^{3/4} \kappa^{3/2} / (k y) \end{aligned} \quad (15)$$

where  $k=0.42$  is the von Kármán constant,  $E=9.793$  is an empirical constant,  $\tau_w$  is the wall shear stress,  $u^*$  is the friction velocity, and  $u^+$  and  $y^+$  are dimensionless velocity and distance.

The non-equilibrium wall function dependent on the pressure gradient is

$$\begin{aligned}
\hat{u} &= (1/k) \ln(E \hat{y}) & \hat{u} &= (\tilde{u}/u_\tau)(u^*/u_\tau) & u^* &= C_\mu^{1/4} \kappa^{1/2} \\
\tilde{u} &= u - \frac{1}{2} \frac{dp}{dx} \left[ \frac{y_\nu}{\rho k \sqrt{\kappa}} \ln\left(\frac{y}{y_\nu}\right) + \frac{y - y_\nu}{\rho k \sqrt{\kappa}} + \frac{y_\nu^2}{\mu} \right] & \hat{y} &= \rho u^* y / \mu & y_\nu &= \hat{y} \mu / (\rho u^*)
\end{aligned} \tag{16}$$

The turbulent kinetic energy equation at the wall-neighboring cells were solved assuming a two-layer concept, i.e., a viscous sublayer and a fully turbulent layer, defined as

$$\tau_t = \begin{cases} 0, & y < y_\nu \\ \tau_w, & y > y_\nu \end{cases} \quad \kappa = \begin{cases} (y/y_\nu)^2 \kappa_P, & y < y_\nu \\ \kappa_P, & y > y_\nu \end{cases} \quad \varepsilon = \begin{cases} (2\nu\kappa)/y^2, & y < y_\nu \\ \kappa^{3/2}/(C_\ell y), & y > y_\nu \end{cases} \tag{17}$$

where  $C_\ell = k C_\mu^{-3/4}$ . Using these profiles, the production of  $\kappa$  and  $\varepsilon$  at the near wall cell were determined by

$$G_\kappa = \frac{1}{y_n} \int_0^{y_n} \tau_t \frac{\partial u}{\partial y} dy = \frac{\rho}{k} \frac{u_\tau^4}{y_n u^*} \ln\left(\frac{y_n}{y_\nu}\right) \quad \varepsilon_P = \frac{1}{y_n} \int_0^{y_n} \varepsilon dy = \frac{\kappa_P}{y_n} \left[ \frac{2\nu}{y_\nu} + \frac{\kappa_P^{1/2}}{C_\ell} \ln\left(\frac{y_n}{y_\nu}\right) \right] \tag{18}$$

where  $y_n$  is the cell height ( $y_n = 2 y_p$ ).

The last model examined was the  $\kappa$ - $\omega$  model of Wilcox, where the turbulent viscosity is

$$\mu_t = \alpha^* \rho \kappa / \omega \quad \alpha^* = \alpha_\infty^* \left( \frac{\alpha_o^* + \mathbf{Re}_t / R_\kappa}{1 + \mathbf{Re}_t / R_\kappa} \right) \quad \mathbf{Re}_t = \frac{\rho \kappa}{\mu \omega} \quad R_\kappa = 6 \quad ; \quad \alpha_\infty^* = 1 \tag{19}$$

$$\alpha_o^* = \beta_i / 3 \quad ; \quad \beta_i = 0,024$$

The  $\kappa$  equation is the same as the  $\kappa$ - $\varepsilon$  model, and the  $\omega$  equation is

$$\frac{\partial}{\partial x_i} (\rho \omega \bar{u}_i) = \frac{\partial}{\partial x_j} \left[ \left( \mu + \frac{\mu_t}{\sigma_\kappa} \right) \frac{\partial \omega}{\partial x_j} \right] + \alpha \frac{\omega}{k} G_k - \rho \beta_i f_\beta \omega^3 \tag{20}$$

$$f_\beta = \frac{1+70 \chi_\omega}{1+80 \chi_\omega} \quad \chi_\omega = \left| \frac{\Omega_{ij} \Omega_{jk} S_{ki}}{(\beta_\infty^* \omega)^3} \right| \quad \alpha = \frac{\alpha_\infty}{\alpha^*} \left( \frac{\alpha_o + \mathbf{Re}_t / R_\omega}{1 + \mathbf{Re}_t / R_\omega} \right) \tag{21}$$

$$\begin{aligned}
R_\omega &= 2,95 \\
\alpha_o &= 1/9 \\
\alpha_\infty &= 0,52 \\
\beta_\infty^* &= 0.09
\end{aligned}$$

### 3. Numerical. Method

The commercial software Fluent was employed to test the models. It is based on the finite volume method (Patankar 1980). The ‘‘Power-law’’ interpolation scheme was selected, and the pressure-velocity coupling was handled by SIMPLE algorithm. A uniform mesh of 200x120 was employed in the  $x$  and  $y$  directions as illustrated in Fig. 2.

For the convergence of the numeric solution, the residues of the mass and momentum conservation equations, as well as the equations of the turbulent models were controlled. The solution was considered converged when the residue was inferior to  $10^{-10}$ .

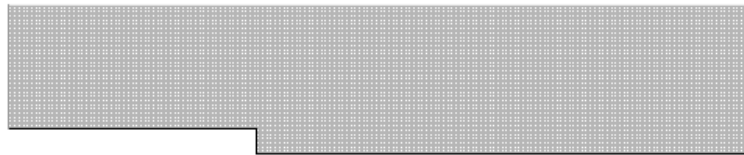


Figure 2. Mesh distribution

### 4. Discussion of the Results

The solution obtained with the six turbulence models for the time average velocity profile, Reynolds stress, pressure and

friction coefficients, were compared with experimental data and Direct Numerical Simulation (DNS) data of Le et al. (1997).

The pressure coefficient  $C_p$  and the friction coefficient  $C_f$  were defined as

$$C_p = (p - p_o) / (\rho U_o^2) \quad C_f = \tau_w / (0.5 \rho U_o^2) \quad (22)$$

where  $p_o$  is the pressure at the inlet channel center line and  $\tau_w$  is the wall shear stress. A comparison among the results obtained with all models for the pressure coefficient and friction factor is presented in Figures 3 and 4.

Figure 3 presents the pressure coefficient distribution along the lower wall. All models super estimated the pressure at the recirculation region, but predicted reasonable well the pressure level near the exit. The only exception was the Spalart-I, which showed a smaller pressure level. It can be seen that the  $\kappa$ - $\epsilon$  family models anticipated the pressure recovery. The standard  $\kappa$ - $\epsilon$  model with the non-equilibrium wall law ( $\kappa$ - $\epsilon$  I) presented the worst pressure recovery prediction. Both Spalart Allmaras models underestimated the pressure at the recirculation zone, but presented a good pressure recovery. The best agreement with the experimental and DNS results was obtained with  $\kappa$ - $\omega$  model.

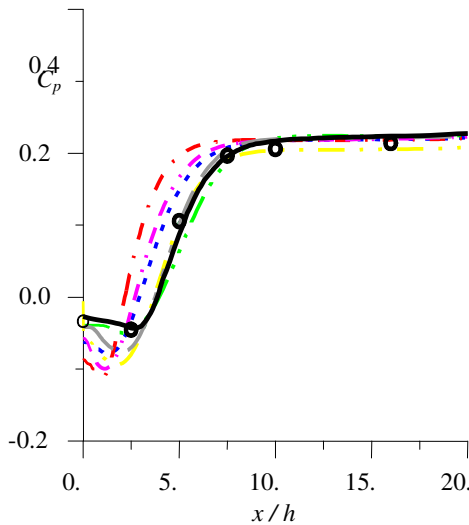


Figure 3. Pressure coefficient:  
 experimental o o o o DNS ——— (Le at al, 1997)  
 $\kappa$ - $\epsilon$ -I - - - -  $\kappa$ - $\epsilon$ -II - - - -  $\kappa$ - $\omega$  - - - -  $\kappa$ - $\epsilon$ -RNG - - - - Spalart I - - - - Spalart II - - - -

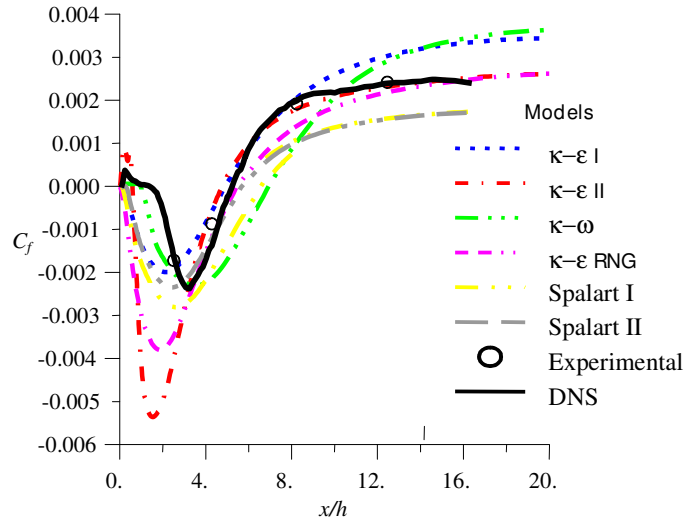


Figure 4. Friction coefficient:

The friction coefficient distribution along the bottom wall (fig. 4) helps to determine the zones of primary and secondary recirculation, by analyzing the change of sign of the stress along the bottom wall. The results obtained for the reattachment distance  $x/h$  for each model were: for  $\kappa$ - $\epsilon$ -I=4,7;  $\kappa$ - $\epsilon$ -II=4,73;  $\kappa$ - $\epsilon$ -RNG=5.32;  $\kappa$ - $\omega$ =6.96; Spalart-I=7.00 and Spalart-II=7.00; while the DNS results are  $x/h$ =6.75. Once again, the worst result was obtained with  $\kappa$ - $\epsilon$ -II, but it was the only one that captured the secondary recirculating region. All  $\kappa$ - $\epsilon$  models, underestimate the size of the main recirculating zone, with large negative stress in the recirculating region. The best prediction for the reattachment point corresponds to the  $\kappa$ - $\omega$  model. The three  $\kappa$ - $\epsilon$  models predicted very small recirculating region, and large negative stress in the recirculating region. The results of the two Spalart Allmaras models are very similar, indicating that the mayor contribution to the viscosity is the vorticity.

#### 4.1. Time Average Velocity Profiles

The velocity profiles at different axial coordinates are presented in Fig. 5. Figure 5a. corresponds to the axial position  $x/h = 0.5$ , while fig. 5b, 5c, 5d and 5e correspond respectively to  $x/h$  equal to 1; 4; 6 and 10. It can be said that in general, a good agreement between the solutions were obtained in the core region for all models. However, near the step, in the recirculation zones, there is some discrepancy among the results. Very close to the step (Fig. 5a and 5b) larger negative velocity can be seen for almost all models. Model  $\kappa$ - $\epsilon$  II shows larger negative velocities in the recirculation zone. It also shows a faster development. A better prediction of the negative velocities in the recirculation region was obtained with the  $\kappa$ - $\omega$  model, in agreement with the previous results. Far from the step, all models present a similar result with a small over predicting of the velocity near the wall.

In the recirculation zone, the  $\kappa$ - $\epsilon$  I and  $\kappa$ - $\epsilon$  II models failed to obtain the correct solution, showing a tendency to smooth the curves in the regions far from de wall. This might indicate that the turbulence diffusion is being overestimated by the models, which reflects directly on the reattachment distance prediction.

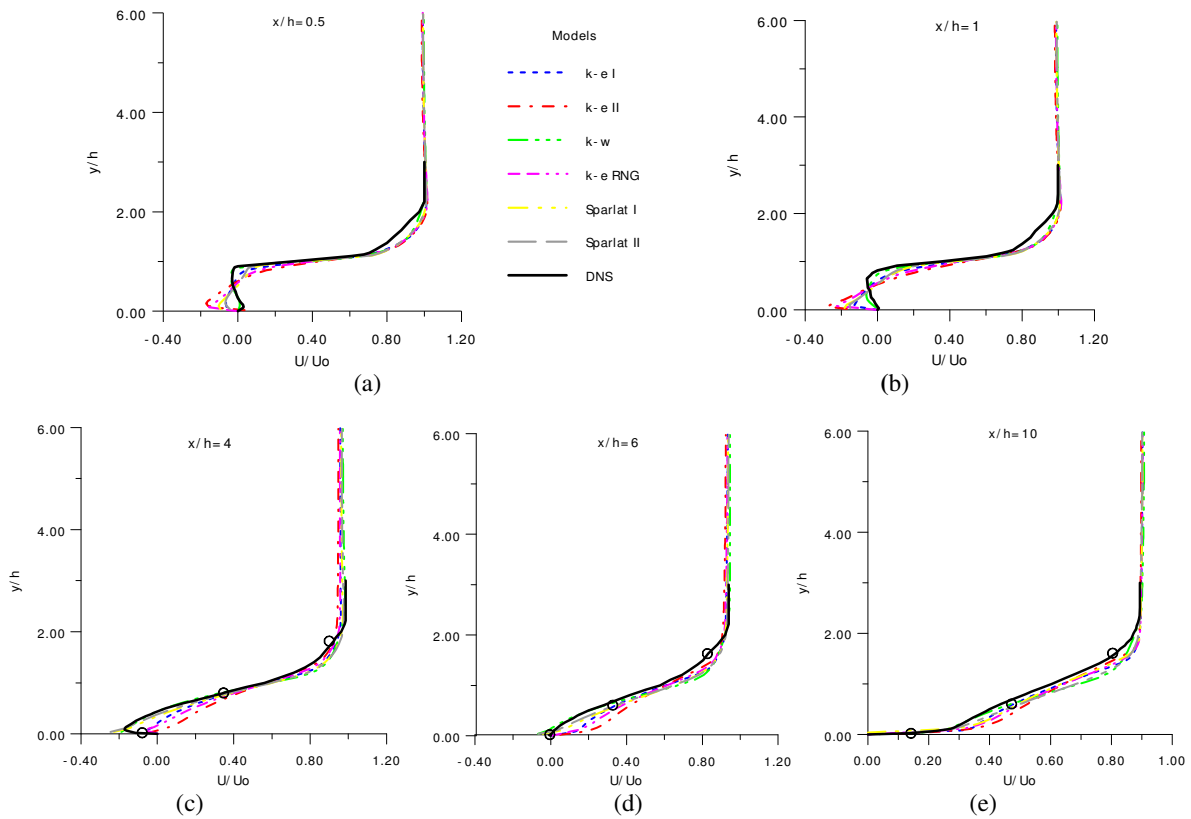


Figure 5. Time average velocity profile at different axial positions: experimental  $\circ \circ \circ \circ$  DNS  $\text{—}$   
 $\kappa\text{-}\epsilon\text{-I}$   $\text{---}$   $\kappa\text{-}\epsilon\text{-II}$   $\text{---}$   $\kappa\text{-}\omega$   $\text{---}$   $\kappa\text{-}\epsilon\text{-RNG}$   $\text{---}$  Spalart I  $\text{---}$  Spalart II  $\text{---}$

## 4.2. Reynolds Stress

Figures 6 and 7 present a comparison of the results for the normal component stress  $\overline{u^2u'}$  with experimental and DNS data, at three different axial positions. Figure 6 corresponds to results obtained with the  $\kappa\text{-}\epsilon\text{-I}$ ;  $\kappa\text{-}\epsilon\text{-II}$  and  $\kappa\text{-}\omega$  models for  $\sqrt{\overline{u'u'}}/U_0$  while fig. 7 corresponds to the results of  $\overline{u^2u'}/U_0^2$  obtained with  $\kappa\text{-}\epsilon\text{-RNG}$ , Spalart I and Spalart II models. The selected sections were  $x/h$  are 4, 6 and 10. By examining fig. 6, it can be seen that all models were able to capture the qualitative behavior of the normal stress; however, slightly smaller values were predicted. The results of  $\kappa\text{-}\epsilon\text{-I}$  and  $\kappa\text{-}\epsilon\text{-II}$  models presented good agreement with the DNS data at  $x/h=4$ , but further downstream it diminishes faster than the experimental data. Note that while the best results for the average variables (velocity, pressure, friction) were obtained with  $\kappa\text{-}\omega$  models, the results of the turbulent quantities were underestimated. The  $\kappa\text{-}\omega$  model predicted practically the same profile for the normal Reynolds stress, at the three sections. Further, it can be seen that the three models presented an equal, non-zero normal turbulent stress at the core region.

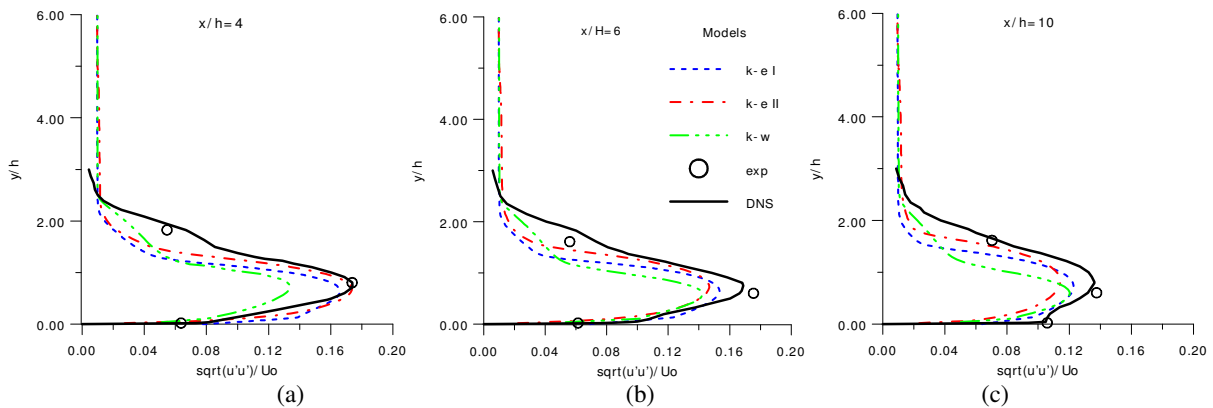


Figure 6. Turbulent shear stress  $\overline{u^2u'}$ .  
 $\kappa\text{-}\epsilon\text{-I}$   $\text{---}$   $\kappa\text{-}\epsilon\text{-II}$   $\text{---}$   $\kappa\text{-}\omega$   $\text{---}$  experimental  $\circ \circ \circ \circ$  DNS  $\text{—}$

The results of Spalart I, Spalart II and  $\kappa$ - $\epsilon$  RNG are presented separately in fig. 7, because the normal Reynolds stress showed negative values, which is physically impossible. This should reinforce the idea that all models count with a heuristic approach for the closure problem. To understand this result, it is convenient to recall that there are no turbulent kinetic energy contributions to the Reynolds Stress in the Spalart Allmaras models. The Spalart Reynolds stress models is evaluated by  $\overline{u'u'} = -2\nu_t(\partial\bar{u}/\partial x)$ . Thus the stress sign depends directly on the velocity gradient. Near the wall, the stress has the correct sign, but at the central region unrealistic results were obtained. The Spalart models and  $\kappa$ - $\epsilon$  RNG predicted the correct level of the turbulent normal stress at the recirculation region, but all models predicted a faster decay of  $\overline{u'u'}$  than the experimental data, indicating that dissipation is larger than it should be.

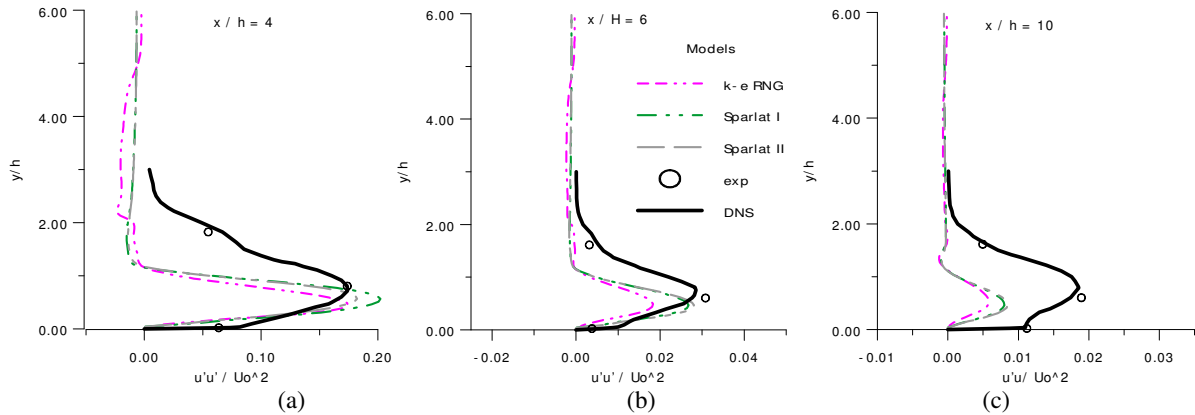


Figure 7. Turbulent shear stress  $\overline{u'u'}$ .

$\kappa$ - $\epsilon$ -RNG - - - Spalart I - - - Spalart II - - - experimental o o o o DNS —

The turbulent shear stress  $\overline{u'v'}$  dimensionized by  $U_o^2$  is presented at Fig. 8, for all six models at the same sections as the previous results. In general, these are one order of magnitude smaller than the normal stress  $\overline{u'u'}$ . Comparing the results obtained with the experimental and DNS data, it was observed that in general the agreement between the solutions is good. However, the traditional  $\kappa$ - $\epsilon$ -I model with the wall law and the  $\kappa$ - $\omega$  model presented a peak on the turbulent shear stress which is not present in the experimental and DNS data.

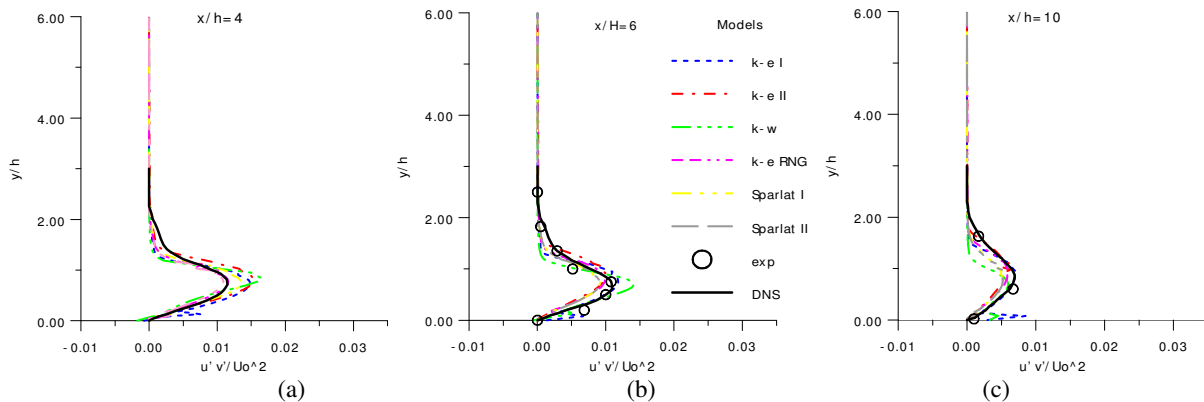


Figure 8. Turbulent shear stress  $\overline{u'v'}$ : experimental o o o o DNS —

$\kappa$ - $\epsilon$ -I - - -  $\kappa$ - $\epsilon$ -II - - -  $\kappa$ - $\omega$  - - -  $\kappa$ - $\epsilon$ -RNG - - - Spalart I - - - Spalart II - - -

## 5. Conclusion

The performance of the traditional  $\kappa$ - $\epsilon$  with two different wall treatment ( $\kappa$ - $\epsilon$ -I and  $\kappa$ - $\epsilon$ -II), the  $\kappa$ - $\epsilon$  RNG, the  $\kappa$ - $\omega$  model and two variation of the Spalart Allmaras models (Spalart I and Spalart-II) in a backstep geometry was analyzed and comparison was done with available experimental and direct numerical simulation data.

The results showed that in general the best agreement among the numerical results for the time average quantities and the experimental data was obtained with the  $\kappa$ - $\omega$  model. The results obtained with the traditional  $\kappa$ - $\epsilon$ -I showed a faster decrease on the intensity of Reynolds tensor when compared with the DNS data, indicating that the models are too dissipative. The Spalart Allmaras models as well as the  $\kappa$ - $\epsilon$  RNG model over predicted the velocity profile. The best result

for the turbulent quantities was obtained with  $\kappa$ - $\epsilon$ -II, but this same model predicted the worst time average results.

The Spalart Allmaras models presented negative values for the Reynolds stress component  $\overline{u' u'}$ , indicating that this model does not present reasonable results for this type of problem. This result may be explained if we recall that for these models, the turbulent viscosity does not depend on the turbulent kinetic energy. The Reynolds stress is just function of the turbulent viscosity, velocity gradients and transpose velocity gradient while the others take in account the turbulent kinetic energy. Note that in abrupt expansion convective reacceleration seems be reasonable.

By analyzing the results, it can be concluded that no model presented a very good result, however if a compromised decision has to be made, the best combined result for the time average and turbulent quantities was obtained with the  $\kappa$ - $\omega$  model, which can be recommended.

## 6. Acknowledgement

The authors acknowledge support from CNPq.

## 7. References

- Avancha, R.V.R. and Pletcher, R.H., 2002, "Characterization of a coupled phenomenon in a confined shear-layer", Int. Journal of Heat and Fluid Flow, pg 601.
- Bredberg, J., Peng, S., And Davidson, L., 2002, An Improved  $\kappa$ - $\epsilon$  Turbulence Model Applied To Recirculating flows, International Journal Heat and Fluid Flow, Vol. 23, No. 6, pp. 731-743.
- Kung et al, 2003
- Eaton, J.K., and Johnston, J.P., 1981, "A Review of Research on Subsonic Turbulent Flow Reattachment," AIAA J., 19, No. 9, pp. 1093-1100.
- Lee, T. and Mateescu, D., 1998, "Experimental and numerical study of 2-D backward-facing step flow," Journal of Fluids and Structures, Vol. 12, pp. 1-14.
- Spalart, P., R., and Allmaras, S., R., 1992, "A One-Equation Turbulence Model For Aerodynamic Flows", Technical Report AIAA-92-0439, American Institute of Aeronautics and Astronautics
- Jovic, S., and Driver, D., 1994, 'Backward-Facing Step Measurement At Low Reynolds Number'. NASA Tech. Mem. 108807;
- Jones, W. P., and Launder, B. E., 1972, The prediction of laminarization with two-equations model of turbulence, Int. J. Heat Mass Transfer, vol. 15, pp. 301-314;
- Kim, S-E and Choudhury, D., 1995, "A Near-Wall Treatment Using Wall Functions Sensitized to Pressure Gradient", ASME FED Vol. 217, Separated and Complex Flows. ASME
- Le, H., Moin, P., and Kim, J., 1997, Direct numerical simulation of turbulent flow over a backward facing step, J. Fluid Mech., vol. 330, pp.349-374;
- Patankar, S. V., 1980, "Numerical Heat Transfer e Fluid Flow", McGraw-Hill;
- Silveira Neto, A., Grand, D., et, Lesieur, M., 1993, "A Numerical Investigation Of Coherent Structures Of Turbulence Behind A Backward-Facing-Step", J. Fluid Mech., Vol. 256
- Silveira Neto, A., 2002, "Fundamentos da Turbulência Nos Fluidos" Terceira escola de turbulência, Florianópolis, SC, Brasil;
- Tylli, N., Kaiktsts, L., Ineichen, B., 2002, "Sidewall effects in flow over a backward-facing step: Experiments and numerical simulations", Physics of Fluids, Vol. 14, No. 11, pp. 3835, 3845.
- Wilcox, D. C., 1988, "Reassessment of The Scale-Determining Equation For Advanced Turbulence Models", AIAA Journal, Vol. 26;

## 8. Copyright Notice

The authors are the only responsible for the printed material included in his paper..